Revisiting tolerance to ocean acidification: insights from a new framework combining physiological and molecular tipping points of Pacific oyster

Mathieu Lutier[1,*], Carole Di Poi[1], Frédéric Gazeau[2], Alexis Appolis[1], Jérémy Le Luyer[3], Fabrice Pernet[1,*]

[1] LEMAR CNRS/UBO/IRD/Ifremer, ZI pointe du diable, CS 10070, F-29280 Plouzané, France.

[2]LOV Sorbonne Université, CNRS, Laboratoire d'Océanographie de Villefranche, Villefranche-sur-Mer, France.

[3]EIO UPF/IRD/ILM/Ifremer, Labex CORAIL, Unité RMPF, Centre Océanologique du Pacifique, Vairao – BP 49 Vairao, Tahiti, Polynésie française.

Correspondence and requests for materials should be addressed to M.L. (email: mathieu.lutier@gmail.com) or to F.P. (email: fpernet@ifremer.fr)

For submission to global change biology.

Abstract

Studies on the impact of ocean acidification on marine organisms involve exposing organisms to future acidification scenarios as projected for open ocean, which has limited relevance for coastal calcifiers. Characterization of reaction norms across a range of pH and identification of tipping points beyond which detrimental effects are observed has been limited and focus on only a few macro-physiological traits. Here we filled this knowledge gap by developing a framework to analyze the broad macro-physiological and molecular responses over a wide pH range of juvenile Pacific oyster, a model species for which the tolerance threshold to acidification remains unknown. We identify low tipping points for physiological traits at pH 7.3-6.9 that coincide with a major reshuffling in membrane lipids and transcriptome. In contrast, shell parameters exhibit effects with pH drop well before tipping points, likely impacting animal fitness. These findings were made possible by the development of an innovative methodology to synthesize and identify the main patterns of variations in large -omic datasets, fit them to pH and identify molecular tipping-points. We propose the application of our framework broadly to the assessment of effects of global change on other organisms.

Keywords

Acidification, Lipidomic, Mollusk, Reaction norm, Threshold, Transcriptomic

Introduction

The exponential increase in the atmospheric emission of carbon dioxide (CO_2) from anthropogenic activities is mitigated by ocean absorption that leads to decreasing surface ocean pH and changes in carbonate chemistry, a phenomenon known as ocean acidification (OA) (Caldeira & Wickett, 2003; Orr et al., 2005). This represents a tremendous challenge for marine organisms, especially for calcifiers that produce calcium carbonate ($CaCO_3$)-based exoskeletons. OA not only induces internal acidosis that impacts metabolism, behavior, growth and reproduction, but also decreases carbonate ions (CO_3^{2-}) concentration in the ocean, the elemental constituent of calcifier exoskeletons (Gazeau et al., 2013; IPCC, 2019; Kroeker et al., 2013; Tresguerres & Hamilton, 2017).

OA has been the most-studied topic in marine science in recent times (Browman, 2017). As such, many OA experiments have been conducted, usually exposing organisms to experimental conditions based on scenarios modelled for open ocean waters, typically simulating present and near-future surface ocean pH levels. However, many calcifying species thrive in coastal areas where pH levels vary far more than in the open ocean on both daily and seasonal scales (Vargas et al., 2017; Waldbusser & Salisbury, 2014). Such variability in coastal environments limits the relevance of applying projections based on simulations for the open ocean and indicates that knowing the physiological response of coastal organisms over a wider pH range (Dorey et al., 2013) would be necessary to accurately assess OA impact.

Reaction norm, i.e. the response of an organism to changing environmental parameters, allows the identification of tipping points that beyond small variations will have major impacts. According to the last IPCC reports, identification of tipping-points is a key knowledge gap in environmental change research (IPCC, 2019, 2021). To date,

only four studies have experimentally established reaction norms for marine calcifiers in relation to pH. These studies focused on the assessment of tipping points for a few selected traits measured at the organism level (i.e. growth, survival) and provide a limited view of the whole organism response, ignoring the molecular level (Comeau et al., 2013; Dorey et al., 2013; Lee et al., 2019; Ventura et al., 2016). We therefore identify the need to integrate macro-physiology and omics together with the reaction norm for understanding the mechanisms responsible for individual organism success under a changing environment. This however requires developing an innovative methodology to synthesize and identify the main patterns of variations in large -omics datasets (Strader et al., 2020) and fit them to reaction norm.

Transcriptomic and lipidomic approaches provide holistic views of organismal responses to environmental changes at the molecular and biochemical levels. Organisms do vary in their transcriptomic responses to pH but common patterns have been observed, including shifts in acid-base ion regulation, metabolic processes, calcification and stress response mechanisms (Matz, 2018; Strader et al., 2020). Membrane composition in terms of fatty acid is also modulated as a response to environmental changes and influence exchanges between intra and extracellular compartments with impacts on metabolic rates (Hazel & Williams, 1990; Hochachka & Somero, 2002; Hulbert & Else, 1999).

Here we determine the reaction norm of juvenile Pacific oyster *Crassostrea gigas*, one of the most cultivated invertebrate species in the world (FAO, 2020), over a wide range of pH for macro-physiological traits, membrane lipids and gene expression. Although the impacts of OA on this model species have been intensively studied using scenario approaches, there is currently no consensus on its robustness to low pH (Ducker & Falkenberg, 2020). The establishment of reaction norm with biochemical and

molecular data is a novel approach that provide new insights on the sensitivity of marine calcifiers to OA.

Material and methods

Animals and maintenance

The oysters were produced at the Ifremer hatchery facilities in Argenton (Brittany, France) in late August 2018 according to Petton et al. (2015). The broodstock consisted of 139 females and 40 males originating from six different cohorts collected in the natural environment between 2011 and 2016, off Fouras (Ile d'Aix, France). At 40 days old, the juveniles were moved to the Ifremer growing facilities in Bouin (Vendée, France). On January 10th 2019, oysters were returned to Argenton and kept for 8 d in a 500 L flow-through tank. Seawater temperature was gradually increased from 7 °C to 22 °C, the optimal temperature for *C. gigas* (Bayne, 2017), at a rate of *ca*. 2 °C d^{-1}. During the experiment, oysters were continuously supplied with natural seawater originating from a pool (~9000 m^3) which is renewed with each spring tide, filtered at 5 µm and UV-treated. The oysters were fed continuously on a mixed diet of *Isochrysis affinis galbana* (CCAP 927/14) and *Chaetoceros gracilis* (UTEX LB2658) (1:1 in dry weight). Food concentration was maintained at 1500 µm^3 mL^{-1} of phytoplankton cells at the outlet of the tank – *ad libitum* (Rico-Villa et al., 2009) – and controlled twice daily using an electronic particle counter (Multisizer 3, Beckman Coulter, USA) equipped with a 100 µm aperture tube. On the eve of the experiment on January 14th 2019, oysters were 5-month-old and divided into 15 batches containing 292 ± 20 individuals (95.2 ± 0.2 g).

Experimental design

Each batch of oysters was exposed to one constant nominal pH condition ranging from pH 7.8 to 6.4 with a step of 0.1 between two levels. The upper pH condition (pH

~7.8) was obtained by running seawater with oysters without pH regulation. The experimental system consisted of 18 experimental units that were randomly assigned to one pH condition (n = 15) or to control blanks without animals (n = 3). Each experimental units consisted of a header tank in which seawater was acidified (except for the ambient pH and blanks) and then delivered by a pump to a holding tank containing the oysters. These tanks were 45 L and their entire volume was renewed every 82 min. pH was regulated by means of pure-CO_2 bubbling, controlled by a pH-regulator (ProFlora® u403 JBL). The pH-regulator was connected to pH-probes installed in each header tank (pH-sensor+Cal, JBL), checked at the start of the experiment using Certipur® Merck NBS buffers (pH = 4.00, pH = 7.00). pH electrodes from the pH-regulator were inter-calibrated twice daily against a pH probe (Sentix® 940-3 WT) connected to a Multiline® Multi 3630 IDS-WTW. The pH-probe was checked once a week using Certipur® Merck NBS buffers (pH = 4.00, 7.00, and 9.00) and calibrated twice a week on the total scale with a certified Tris/HCl buffer (salinity 35; provided by A. Dickson, Scripps University, USA). Throughout the text, pH levels are therefore expressed on the total scale (pH_T). In each experimental tank, air bubbling and a small homogenisation pump (3 W) ensured an efficient mixing of seawater surrounding the oysters. Photoperiod was 10 h light: 14 h dark. During the entire experimental period, oysters were fed as described above.

On January 18th 2019, each batch of oyster was randomly assigned to one tank. Oysters were first held at ambient pH for 3 d. Then, pH was progressively decreased in each pH-regulated tank at a rate of 0.2 unit d^{-1}. The decrease in pH lasted for 7 d for the lowest condition. Experimental pH conditions were all reached on January 27th 2019 and oysters were maintained at these experimental pH levels for 23 d. No mortality was recorded during the experiment.

138 **Seawater carbonate chemistry**

139 In each oyster tank, temperature, salinity, dissolved oxygen (O_2) saturation levels
140 and pH were measured twice a day using a Multiline® Multi 3630 IDS-WTW (pH probe
141 Sentix® 940-3 WTW, O_2 probe FDO® 925 WTW, salinity probe TetraCon® 925 WTW).
142 Seawater samples were collected weekly, filtered on 0.7 µm (GF/F, Whatman®) and
143 poisoned with 0.05% mercury (II) chloride. Total alkalinity (TA) was then measured in
144 triplicate 50 mL subsamples by potentiometric titration at 22 °C, using a Titrando 888
145 (Metrohm®) titrator coupled to a glass electrode (ecotrode plus, Metrohm®) and a
146 thermometer (pt1000, Metrohm®). TA was calculated following the protocol described in
147 Dickson et al. (2007). pH and TA, together with salinity and temperature, were used to
148 determine carbonate chemistry parameters using the package seacarb v 3.2.16. of the R
149 software.

150 **Biometry**

151 The total fresh weight (shell + tissue) of each batch of oysters was measured twice
152 weekly and interpolated between measurements to estimate daily weight. In addition,
153 shell length and total fresh weight were measured individually on 30 oysters from each
154 condition at the onset (1 d) and at the end of the experiment (23 d). These oysters were
155 then dissected and pooled to determine the total weight of shell and tissue, separately.
156 The tissues were then lyophilized and weighted to obtain dry weight. Growth rate was
157 calculated as:

158 $$G = \left(\overline{X_{23}} - \overline{X_1}\right) \div 23,$$

159 where G is growth rate as expressed as increase in shell length or total body weight per
160 day (mm d^{-1}, g d^{-1}), $\overline{X_1}$ and $\overline{X_{23}}$ are the average parameter values for shell length and total
161 weight measured at the onset (1 d) and the end of the experiment (23 d).

Shell thickness was measured on the left valve of five individuals collected per pH condition at the end of the experiment. The left valve was more susceptible to acidification than the right valve. We observed holes in the shell under low pH condition (pH < 6.6) that always occurred on the left valves, close to the umbo. Shells were dried for 24 h at 45 °C, embedded in polyester resin and cross-sectioned from umbo to opposite shell margin along the longitudinal growth axis using a precision saw (Secotom-10 Struers). Sections were glued on a microscope slide and polished with silicon carbide abrasive disks (1200 and 2500 grains cm^{-2}). Images of the section were captured under a Lumar V12 stereoscope (Zeiss) at 30x magnification, and the entire section was reconstructed using an image acquisition software (AxioVision SE 64 – v4.9.1, Zeiss). The minimal shell thickness was measured within the first third of the shell starting from umbo using ImageJ software (Schneider et al., 2012).

Physiological rates

Seawater was sampled twice a day at the inlet and outlet of each oyster tank and phytoplankton cell concentrations were measured using an electronic particle counter (see previous section). No pseudofaeces production was detected throughout the experiment. Ingestion rate was determined as:

$$I = \frac{\Delta_{\text{phyto}} \times \text{flow rate}}{W},$$

where I is the ingestion rate expressed as $cm^3\ min^{-1}\ g^{-1}$, Δ_{phyto} is difference in phytoplankton concentrations between the inlet and the outlet of the oyster tanks ($cm^3\ min^{-1}$), *flow rate* is the water flow at the inlet of the oyster tanks ($mL\ min^{-1}$), and W is the total fresh weight of oyster batch (g). The three control blanks were used to check that there was no sedimentation of algae (no differences in cell concentrations between the inlet and the outlet, data not shown).

186 Net calcification and respiration rates were measured after 22 d of exposure. Food
187 supply was stopped 17 h before the assay and tanks were emptied, cleaned and refilled.
188 Again, 1 h before the assay, the tanks were emptied, cleaned and refilled. At the onset of
189 the incubation, water flow and air bubbling were stopped. Gentle mixing of the seawater
190 was maintained by homogenization pump but air bubbling was stopped. Incubations
191 lasted for 90 min. This duration allowed to keep the pH close to the setpoint (< 0.1 pH
192 unit variation) despite oyster respiration. At the onset and at the end of the incubation
193 period, temperature, salinity, pH and O_2 concentration (mg L^{-1}) were measured, and
194 seawater samples were filtered and poisoned for TA analyses (see above) or were
195 immediately frozen at -20 °C for ammonium (NH_4^+) measurements (Aminot & Kérouel,
196 2007) (see Supplementary Table 4). Empty tanks were used as controls to check that there
197 was no change in any of the parameters due to evaporation or other potential biological
198 processes in the water itself. Net calcification rate was determined following a modified
199 procedure from Gazeau et al. (2015) using the alkalinity anomaly technique (Smith &
200 Key, 1975):

201 $$NC = \frac{(\Delta_{TA} \times \rho - \Delta_{NH_4^+}) \times V}{2 \times t \times W \times \frac{DW}{TW}},$$

202 where *NC* is the net calcification rate expressed as μmol $CaCO_3$ h^{-1} g^{-1}, Δ_{TA} and Δ_{NH4+} are
203 differences in TA (μmol Kg^{-1}) and NH_4^+ (μmol L^{-1}) between the onset and the end of the
204 incubation period, ρ is seawater density (kg L^{-1}) calculated based on temperature and
205 salinity during the incubation, *V* is the volume of the tanks (L), *t* is the duration of the
206 incubations (h), $\frac{DW}{TW}$ is the ratio of dry weight and total weight determined after
207 lyophilization of a pool of tissues from 30 oysters (see above).
208 Respiration rate was determined following:

209 $$R = \frac{(\Delta_{O_2} - \Delta_{O_2\ Control} \times \rho) \times V}{t \times W \times \frac{DW}{TW}},$$

where R is the respiration rate expressed as mg O_2 h^{-1} g^{-1}, Δ_{O_2} and $\Delta_{O_2\,Control}$ are differences in O_2 concentration (mg L^{-1}) between the onset and the end of the incubation period in the oyster tank and in the three control tanks (average) respectively.

Biochemistry

Soft-tissues of five individuals from each pH condition were collected at 23 d, flash-frozen in liquid nitrogen, pooled, grounded with a ball mill and stored at -80 °C pending analyses. Oyster powder was diluted with chloroform/methanol (2:1, v/v) for the determination of neutral lipids (triacylglycerol: TAG, and sterols: ST) using high performance thin layer chromatography. TAG-ST ratio was used as a proxy of the relative contribution of lipid reserve to structure (membrane). Polar lipids were purified on silica gel micro column, transesterified using methanolic H_2SO_4 at 100 °C, and the resulting fatty acid methyl esters (FAME) were analyzed using a gas-chromatography flame ionization detection system equipped with a DB-Wax capillary column. Peaks were analyzed by comparison with external standards. Each fatty acid was expressed as the peak area percentage of total polar fatty acids. Carbohydrate content (µg mg^{-1}) was determined according to the colorimetric method described in DuBois et al. (1956).

Transcriptomics

Soft-tissues of five individuals from each tank were collected at 23 d, flash-frozen in liquid nitrogen and individually grounded (n = 75). Total RNA was then extracted with Extract-All (Eurobio) at a ratio of 5 mL per 100 mg of tissue. RNA quantity/integrity and purity were verified with a NanoDrop 2000 spectrophotometer (Thermoscientific®) and a Bioanalyzer 2100 (Agilent Technologies®) respectively. Samples were then DNase-treated using a DNase Max™ Kit (MO BIO Laboratories, Inc.) and analyzed at the Genotoul sequencing platform (INRAE US 1426 GeT-PlaGe, Centre INRAE de Toulouse

Occitanie, Castanet-Tolosan, France). TruSeq RNA libraries were multiplexed and sequenced on a single lane of NovaSeq6000 Illumina S4 150-bp paired-end.

Raw reads were first filtered using Trimmomatic v.0.36 for a minimum length (60 bp), a minimum quality (trailing = 20, leading = 20) and the presence of potential contaminants and remaining adaptors (https://ftp.ncbi.nlm.nih.gov/pub /UniVec; 08/17/20). The quality of the reads was monitored before and after this trimming process with FastQC v.0.11.5 (https://www.bioinformatics.babraham.ac.uk/projects/fastqc/). The *C. gigas* reference genome (Peñaloza et al., 2021) was downloaded from NCBI (GCF_902806645.1) and indexed with Gmap v2020.06.01. Filtered reads were mapped against the reference genome using GSNAP v2020-06-30 keeping default parameters but allowing a minimum mismatch value of 2 and a minimum read coverage of 90%. Finally, the gene expression levels were assessed using HTSEQ v0. 6.1. The DESeq2 v1.30.0 R package was used to process the expression with a first step of normalization using the variance-stabilizing transformation implemented in the *'vst'* function. The *vst* matrix was used to build a signed weighted co-expression network analysis implemented in the WGCNA v1.69 R package. First, genes with low overall variance (< 5%) were removed for the analysis as recommended (Langfelder & Horvath, 2008). We fixed the "soft" threshold powers of 13 the scale-free topology criterion to reach a model fit (|R|) of 0.90. Clusters were defined using the "*cutreeDynamic*" function (minimum of 50 genes by cluster and default cutting height of 0.99) based on the topological overlap matrix, and an automatic merging step with the threshold fixed at 0.25 (default) allowed merging correlated clusters. For each cluster, we defined the cluster membership (kME; Eigengene-based connectivity) and only clusters showing significant correlation ($p < 0.01$) to pH were kept for downstream functional analysis.

354 **Statistical analysis**

355 All statistical analyses were performed using the R software v4.0.3 and the
356 threshold of statistical significance was fixed at 0.05 unless specifically stated.
357 Relationships between dependent variables and average pH recorded during the exposure
358 period (or the incubation period for net calcification and respiration rates) were computed
359 using regression models. Dependent variables were biometrics (shell length, total body
360 weight, and growth), physiological rates (ingestion, net calcification and respiration),
361 biochemistry (lipid reserves, carbohydrates) and gene expression. Each gene included in
362 the WGCNA clusters were individually tested against pH. Fatty acids were summarized
363 using principal component analysis and separated into two groups according to their
364 correlation with first principal component (positive or negative). Each group was then
365 summed and tested against pH. Piecewise, linear and log-linear regression models were
366 tested and compared for each individual variable (or set of variables). In each case, the
367 model that had the highest R^2, the lowest Akaike and Bayesian information criteria (AIC,
368 BIC) and the lowest residual sum of squares was selected. For each piecewise regression
369 model, we estimated the tipping point, defined as the values of the pH where the
370 dependent variables tip, by implementing the bootstrap restarting algorithm (Wood,
371 2001). For physiological rates, we also determined the critical-point defined as the pH at
372 which the dependent variable was equal to zero. Normality of residual distribution was
373 tested using Shapiro-Wilk test and homogeneity of variances was graphically checked.
374 Significance of each slope was tested according to Student's *t* test. Piecewise regression
375 models were built using the segmented v1.3-4 R package.
376 For transcriptomic analysis, only genes that are significantly correlated to pH were tested
377 among the retained clusters (Pearson correlation). The frequency distribution of pH
378 tipping-point values was plotted for each cluster of genes. Groups of genes which exhibit

neighboring tipping points with distribution frequencies > 5%, were grouped together and used for GO enrichment analysis using GOA-tools v0.7.11 (Klopfenstein et al., 2018), implemented in the Github repository '*go_enrichment*' (https://github.com/enormandeau/go_enrichment) and the go-basic.obo database (release 2019-03-19) with Fisher's extract tests. Only significant GO terms that included a minimum of three genes and with Bonferroni adjusted $P < 0.01$ were kept. For complementarity with previous studies, we also specifically examined the genes that are commonly reported as involved in the calcification process and in the formation of the organic matrix of the shell and periostracum.

Results

Acclimation of oysters to 15 different pH conditions

During the experiment, pH levels in the oyster tanks were stable and reached the targeted values, except for the lowest pH condition that was 6.5 ± 0.3 instead of 6.4 (Supplementary Note 1, Supplementary Table 1, Supplementary Figure 1). The effects of acidification were clearly visible at the end of the experiment on the color and the size of the shells, as shown in Figure 1. Shell pigmentation apparently decreased with decreasing pH. Total body weight and shell length of oysters ranged from 0.4 ± 0.1 to 2.0 ± 0.8 g and from 12.9 ± 2.1 to 25.4 ± 4.5 mm respectively (mean ± SD; Figure 2A, Supplementary Figure 2).

Most macro-physiological traits tip at low pH values between 7.1-6.9

We measured biometric parameters like the length, thickness, and weight of the shell and the total body weight and the dry flesh weight at the end of the 23-day exposure to the 15 different pH conditions. We calculated growth rates for shell length and total body weight, and we measured physiological rates like calcification, ingestion and respiration rates. From these data, we identified an overall tipping point for macro-

404 physiological traits at pH ~7.1-6.9 below which they declined sharply (Figures 2A-H).
405 Calcification rate and growth rates exhibited critical points at pH 6.8 and 6.6, respectively,
406 below which they became negative and turned to net dissolution of the shell and weight
407 losses (Figures 2B-D). Concomitantly, respiration rate was arrested at pH 6.7 and
408 ingestion rate was near-zero at pH 6.5 (Figure 2E-F).

409 **Shell parameters and respiration rate are impacted above tipping point**

410 Although macro-physiological traits were generally unaffected by reductions in
411 pH above tipping points, this was not the case for shell length, shell weight and respiration
412 rate. Both shell parameters indeed decreased with decreasing pH while the respiration
413 rate increased before reaching the tipping point (Figures 2A, 2E and 2G). In addition, the
414 shell thickness was the only parameter that decreased linearly over the entire pH range
415 without tipping point (Figure 2I).

416 **A major remodeling of membrane lipids occurs at pH 6.9**

417 To provide an in-depth characterization of the reaction norms at the whole
418 organism level, we aimed to link the oyster reaction norm established for the macro-
419 physiological traits described previously to the molecular responses of oysters. We first
420 analyzed the fatty acid composition of membrane lipids that play an important role in
421 exchanges between intracellular and extracellular compartments. Principal component
422 analysis of all fatty acids showed that the first axis (PC1) alone explained 66% of the total
423 variance in relation to pH (Figure 3A). The set of fatty acids was reduced to two terms
424 defined by the sums of fatty acids that correlated with PC1 either positively or negatively,
425 and each term was plotted against pH (Figure 3B-C). Positively correlated fatty acids
426 mainly consisted of docosahexaenoic acid (DHA, 22:6n-3) and palmitic acid (PA, 16:0)
427 contributing 43% and 14%, respectively, to PC1 (Supplementary Table 2). This group of

fatty acids exhibited a tipping point at pH 6.9, below which their contribution to membrane decreased markedly (Figure 3B) at the benefit of the fatty acids that were negatively correlated with PC1. These negatively correlated fatty acids consisted of arachidonic acid (ARA, 20:4n-6), eicosapentaenoic acid (EPA, 20:5n-3) and non-methylene interrupted fatty acids (22:2NMI$_{i,j}$), which contributed 12%, 6% and 6%, respectively, to PC1 (Figure 3C) (Supplementary Table 2).

Expression of most genes shows tipping points at pH 7.3-6.9

To further assess the molecular effects of pH change, we compared by RNA-seq the transcriptomic responses of oysters exposed to the 15 pH conditions for 23 days. To do this, we first clustered the differentially expressed genes that co-vary together using WGCNA analysis and retained the clusters that were correlated with pH (Supplementary Table 3). Then, we plotted the frequency distribution of pH tipping-point for each cluster of genes (Figure 4). Owing to this original method, we found that 1054 genes, distributed in three clusters, showed linear (or loglinear) or piecewise regression with pH (Supplementary table 3). Among them, 49% showed tipping-points at pH 7.3-6.9 (Figure 4A-C). Expression level of most genes were unchanged between pH conditions down to the pH tipping point, below which it increased for genes in clusters 1 and 2 (Figure 4A-B), or decreased for genes in cluster 3 (Figure 4C). Some genes linearly increased for clusters 1 and 2, or decreased for cluster 3 with decreasing pH.

Gene ontology analysis (GO) showed that most of the genes from cluster 1 (42%) exhibited tipping-points at pH 7.3-6.9 (Figure 4A) and were associated with GO terms corresponding to the regulation of RNA-transcription, cellular metabolism, macromolecule biosynthesis and negative regulation of cell-cell adhesion (Table 1). The expression of another group of genes from cluster 1 (14%) increased linearly (or loglinearly) with decreasing pH and was associated with GO terms corresponding to

GTP-binding, GTPase activity and ribonucleotide metabolism (Table 1). The expression of most of the genes from cluster 2 (44%) exhibited tipping-points at pH 7.3- 7.0, whereas another large group of genes (18%) increased linearly (or loglinearly) with decreasing pH (Figure 4B). These genes were associated with GO terms corresponding to ribosome synthesis, RNA-binding, translation and protein/amino acid synthesis (Table 1). The expression of 62% of the genes from cluster 3 exhibited tipping-points at pH 7.2-6.9 and decreased thereafter (Figure 4C). These genes were associated with GO terms corresponding to ion transport and more specifically to transmembrane cation transport (Table 1).

Expression of genes related to biomineralization are affected by pH

We specifically examined the genes that are commonly reported in the scientific literature as being involved in the calcification process and in the formation of the organic matrix of the shell and periostracum. We found that the expression of 60% of the 38 genes involved in the calcification process that were retained by our models showed pH tipping points between 6.9 and 7.1 (Table 2). These genes encode for calcium-binding proteins, Ca^{2+} signaling pathway, amorphous calcium carbonate-binding proteins and ion transmembrane transporters. Most of these genes decreased below the tipping-point (n = 14) while others increased (n = 8). The expression of genes associated with the regulation of the synthesis of the shell organic matrix and the periostracum (n = 11) generally increased with decreasing pH (Table 2). The relationships were loglinear (n = 3) or piecewise (n = 8).

Among these 38 genes, the family of genes that are the most represented are coding for acetylcholine receptors, monocarboxylate transporters and tyrosinase synthesis (Table 2). The expression of four genes coding for acetylcholine receptors decreased below tipping points at pH 6.9-7.0. The expression of five genes coding for

478 monocarboxylate transporters increased with decreasing pH, and four of them showed pH
479 tipping points between 7.3 and 6.6. The expression of four genes associated to tyrosinase
480 synthesis early increased with decreasing pH and three of them showed tipping points
481 between pH 7.4 and 7.1.

482 **Discussion**

483 Here we provide the first reaction norm of juvenile oyster *C. gigas* assessed by
484 combining macro-physiological traits and micro-molecular characteristics. This novel
485 approach applied to juvenile oysters exposed to a wide range of pH conditions revealed
486 that macro-physiological parameters such as growth, calcification, food intake, and
487 respiration exhibited pH tipping points that coincide with a major reshuffling in
488 membrane lipids and transcriptome that was previously unappreciated, but others like
489 shell parameters seemed uncoupled from global effect (Figure 5). This comprehensive
490 view of the animal response to environment sheds new light on adaptation potential to
491 climate change.

492 We first identify a global tolerance threshold for juvenile *C. gigas* at pH 6.9-7.3,
493 corresponding to the tipping points identified for the majority of the examined
494 parameters. In line with this, several studies based on IPCC scenario assumed the
495 existence of tipping points below pH 7.5-7.4 for growth, calcification and reproduction
496 in oysters and mussels (Boulais et al., 2017; Fitzer et al., 2014; Lannig et al., 2010). Below
497 tipping points, growth, calcification, respiration and feeding rate decreased markedly,
498 likely reflecting increasing maintenance cost up until reaching critical points that are
499 representative of metabolic depression (Michaelidis et al., 2005; Sokolova, 2021).
500 However, these pH tipping points are well below IPCC projections for 2100 and have
501 unlikely been encountered by mollusks since their appearance on earth 500 million years

ago when CO_2 levels were much higher (IPCC, 2019; Krissansen-Totton et al., 2018). Also, oyster populations do not generally experience such low pH conditions in their habitats (https://wwz.ifremer.fr/cocorico2_en/Donnees). Therefore, juvenile oysters appear to be able to cope with near-future OA.

We show here that shell parameters, i.e. thickness, weight and length, were altered as soon as pH decreased from ambient levels, as already reported for many shellfish species (Byrne & Fitzer, 2019). Shell thickness is generally related to shell strength and therefore with protection against predation and resistance to mechanical stress related to wave exposure and aquaculture processes. Thus, moderate acidification increases predation risk of young *C. gigas* through reduction of shell strength (Wright et al., 2018). We also find that respiration rate first increased when pH decreased, suggesting that metabolism was readily impacted. However, body condition (dry flesh weight) and energy reserves (TAG-ST and carbohydrate, Supplementary Figure 3) were not affected by pH, likely because oysters were fed *ad libitum* (Leung et al., 2019; Thomsen et al., 2013). Finally, we report here a linear increase in the expression level of genes related to GTPase activity and GTP binding, which are characteristics of stress response in *Crassostrea* spp. (Yan et al., 2018). Overall, these changes suggest that longer exposure to moderate acidification (above tipping point) could impair overall oyster fitness.

We further show that this reduction in shell parameters was not related to metabolic depression or to changes in net calcification or global gene expression. In contrast, a recent meta-analysis on *C. gigas* suggests that OA induces a reduction in shell thickness that is related to an overall transcriptional change inducing metabolic depression and alteration of calcification rate (Ducker & Falkenberg, 2020). Here we revisit these assumptions and find in agreement with other prior studies that no metabolic

526 disruptions occurred while shell strength decreased at pH 7.3-7.7 (NBS scale) (Timmins-
527 Schiffman et al., 2014; Wright et al., 2018).

528 Concomitantly, a delamination of the periostracum, the organic coat covering the
529 shell was observed at pH levels above tipping point, probably altering shell protection.
530 This was reflected by an increase shell bleaching and increased expression of four genes
531 coding for tyrosinases-like protein. Tyrosinases are involved in periostracum synthesis
532 and the increase in expression of their related genes is often considered as a mechanism
533 to limit the damage to the periostracum and the corrosion of the shell in reaction to OA
534 (Hüning et al., 2013). Delamination of the periostracum due to moderate OA was
535 frequently associated with alteration of shell properties such as weakening and thinning
536 (Alma et al., 2020; Auzoux-Bordenave et al., 2019; Bressan et al., 2014; Coleman et al.,
537 2014; Peck et al., 2016, 2018; Zhao et al., 2020). Our results agree with the idea that OA
538 is more a dissolution problem than a biomineralization problem (Rajan et al., 2021).

539 This investigation of tipping points at the micro-scale also provides new insights
540 on the physiological response of oysters to OA. For the first time, we find a major
541 remodeling of membrane lipids in response to OA and observed a tipping point at pH 6.9.
542 This remodeling consisted of decreasing the long chain PUFA DHA (22:6n-3) that is
543 essential for growth and survival (Knauer & Southgate, 1999; Langdon & Waldock,
544 1981), at the benefit of eicosanoid precursors (ARA, 20:4n-6 and EPA, 20:5n-3) involved
545 in the stress response (Delaporte et al., 2003). Since membrane fatty acid composition
546 influences the activity of transmembrane proteins involved in ion transport (Hazel &
547 Williams, 1990; Hochachka & Somero, 2002), it could also have been related to
548 regulation of acid-base homeostasis and perhaps calcification under OA.

549 In line with this, we find an overall decrease in expression of genes related to
550 cation transmembrane transport below tipping points at pH 6.9-7.2 that can be related to

551 alteration of calcification and acid-base homeostasis (Zhao et al., 2020). Concomitantly,
552 we observe an overall decrease in the expression of genes coding for proteins involved
553 in the regulation of calcification though calcium signaling pathway, calcium homeostasis,
554 calmodulin signaling pathway and regulation of calcium carbonate crystal growth (Feng
555 et al., 2017; Wang et al., 2017; Zhao et al., 2020).

556 In our analysis, we also identify families of genes that must play an important role
557 in oyster response to OA. Among these genes, we identify four genes coding for
558 acetylcholine receptors that are known for regulating and ordering the formation of the
559 shell micro-structure (Feng et al., 2017). We also find five monocarboxylate transporters
560 coding genes, members of a family of proteins that act as co-transporters of protons H^+,
561 that may be involved in the regulation of acid-base homeostasis and calcification process
562 (Tresguerres et al., 2020; Wang et al., 2020). These proteins also co-transport
563 monocarboxylates such as lactate or pyruvate and were reported to be involved in the
564 stress response of oysters through regulation of metabolic pathways (Ertl et al., 2019).

565 In conclusion, we show that juvenile *C. gigas* have a broad tolerance to ocean
566 acidification, exhibiting tipping points around pH 7.3-6.9 for most parameters (Figure 5).
567 Nonetheless, we observe that shell parameters change as soon as pH drops, well before
568 tipping points are reached, suggesting animal fitness is likely to be affected. This thus
569 raises concerns about the future of natural and farmed oyster populations in a high-CO_2
570 world. This new framework for identification of tolerance threshold in organisms
571 represents a breakthrough in the field of global change research. It was made possible by
572 (1) combining reaction norm assessment and thorough molecular and biochemical
573 analyses of animal responses, and (2) developing a procedure to analyze and synthesize
574 omics data measured over an environmental range. We believe that such an integrative
575 and holistic approach could now be applied to other organisms and integrate intra-specific

576 variation, life-stage and other stressors such as temperature, nutrition, pollutants or
577 oxygen levels.

578 **Acknowledgments**

579 We are grateful for K. Lugue, J. Veillet, C. Quéré, V. Le Roy and I. Queau for their
580 participation to data recording and the Ifremer staff for their involvement in oyster and
581 algae production. We thank J. Thebault and E. Dabass for their advices in shell analysis.
582 We are also grateful for G. Le Moullac for project conception and funding. This work
583 was funded by the Ocean Acidification Program of the French Foundation for Research
584 on Biodiversity (FRB - www.fondationbiodiversite.fr) and the French Ministère de la
585 transition écologique.

586 **Author contributions**

587 ML, CDP, and FP designed and conducted the experiment. All authors analyzed the data.
588 ML performed statistics. ML and FP wrote the first draft of the document and all authors
589 contributed and accepted it. FP and JL obtained the funding. This work is part of the PhD
590 thesis of ML.

591 **Data availability**

592 RNA-seq data have been made available through the SRA database (BioProject accession
593 number PRJNA735889). Other data analyzed during this study are included in this
594 published article and its supplementary information files or available through the
595 SEANOE database (https://doi.org/10.17882/83294). Complementary information is
596 available from the corresponding authors on reasonable request.

597 **Competing interests**

598 The authors declare no competing interests.

599 **Bibliography**

600 Alma, L., Kram, K. E., Holtgrieve, G. W., Barbarino, A., Fiamengo, C. J., & Padilla-
601 Gamiño, J. L. (2020). Ocean acidification and warming effects on the physiology,
602 skeletal properties, and microbiome of the purple-hinge rock scallop.
603 *Comparative Biochemistry and Physiology Part A: Molecular & Integrative*
604 *Physiology*, *240*, 110579. https://doi.org/10.1016/j.cbpa.2019.110579

605 Aminot, A., & Kérouel, R. (2007). *Dosage automatique des nutriments dans les eaux*
606 *marines* (MEDD, Editions Quae). Ifremer.
607 https://www.quae.com/produit/924/9782759200238/dosage-automatique-des-
608 nutriments-dans-les-eaux-marines

609 Auzoux-Bordenave, S., Wessel, N., Badou, A., Martin, S., M'Zoudi, S., Avignon, S.,
610 Roussel, S., Huchette, S., & Dubois, P. (2019). Ocean acidification impacts
611 growth and shell mineralization in juvenile abalone (Haliotis tuberculata). *Marine*
612 *Biology*, *167*(1), 11. https://doi.org/10.1007/s00227-019-3623-0

613 Bayne, B. L. (2017). *Biology of Oysters* (Vol. 41). Academic Press.

614 Boulais, M., Chenevert, K. J., Demey, A. T., Darrow, E. S., Robison, M. R., Roberts, J.
615 P., & Volety, A. (2017). Oyster reproduction is compromised by acidification
616 experienced seasonally in coastal regions. *Scientific Reports*, *7*(1), 13276.
617 https://doi.org/10.1038/s41598-017-13480-3

618 Bressan, M., Chinellato, A., Munari, M., Matozzo, V., Manci, A., Marčeta, T., Finos, L.,
619 Moro, I., Pastore, P., Badocco, D., & Marin, M. G. (2014). Does seawater
620 acidification affect survival, growth and shell integrity in bivalve juveniles?
621 *Marine Environmental Research*, *99*, 136–148.
622 https://doi.org/10.1016/j.marenvres.2014.04.009

623 Browman, H. I. (2017). Towards a broader perspective on ocean acidification research.
624 *ICES Journal of Marine Science*, *74*(4), 889–894.
625 https://doi.org/10.1093/icesjms/fsx073
626 Byrne, M., & Fitzer, S. (2019). The impact of environmental acidification on the
627 microstructure and mechanical integrity of marine invertebrate skeletons.
628 *Conservation Physiology*, *7*(1), 62–82. https://doi.org/10.1093/conphys/coz062
629 Caldeira, K., & Wickett, M. E. (2003). Anthropogenic carbon and ocean pH. *Nature*,
630 *425*(6956), 365–365. https://doi.org/10.1038/425365a
631 Coleman, D., Byrne, M., & Davis, A. (2014). Molluscs on acid: Gastropod shell repair
632 and strength in acidifying oceans. *Marine Ecology Progress Series*, *509*, 203–211.
633 https://doi.org/10.3354/meps10887
634 Comeau, S., Edmunds, P. J., Spindel, N. B., & Carpenter, R. C. (2013). The responses of
635 eight coral reef calcifiers to increasing partial pressure of CO2 do not exhibit a
636 tipping point. *Limnology and Oceanography*, *58*(1), 388–398.
637 https://doi.org/10.4319/lo.2013.58.1.0388
638 Delaporte, M., Soudant, P., Moal, J., Lambert, C., Quéré, C., Miner, P., Choquet, G.,
639 Paillard, C., & Samain, J.-F. (2003). Effect of a mono-specific algal diet on
640 immune functions in two bivalve species—Crassostrea gigas and Ruditapes
641 philippinarum. *Journal of Experimental Biology*, *206*(17), 3053–3064.
642 https://doi.org/10.1242/jeb.00518
643 Dickson, A. G., Sabine, C. L., & Christian, J. R. (2007). *Guide to Best Practices for*
644 *Ocean CO2 Measurements* (PICES Special Publication 3). North Pacific Marine
645 Science Organization. https://www.ncei.noaa.gov/access/ocean-carbon-data-
646 system/oceans/Handbook_2007.html

647 Dorey, N., Lançon, P., Thorndyke, M., & Dupont, S. (2013). Assessing physiological
648 tipping point of sea urchin larvae exposed to a broad range of pH. *Global Change*
649 *Biology*, *19*(11), 3355–3367. https://doi.org/10.1111/gcb.12276
650 DuBois, Michel., Gilles, K. A., Hamilton, J. K., Rebers, P. A., & Smith, Fred. (1956).
651 Colorimetric Method for Determination of Sugars and Related Substances.
652 *Analytical Chemistry*, *28*(3), 350–356. https://doi.org/10.1021/ac60111a017
653 Ducker, J., & Falkenberg, L. J. (2020). How the Pacific Oyster Responds to Ocean
654 Acidification: Development and Application of a Meta-Analysis Based Adverse
655 Outcome Pathway. *Frontiers in Marine Science*, *7*(7), 398–408.
656 Ertl, N. G., O'Connor, W. A., & Elizur, A. (2019). Molecular effects of a variable
657 environment on Sydney rock oysters, Saccostrea glomerata: Thermal and low
658 salinity stress, and their synergistic effect. *Marine Genomics*, *43*, 19–32.
659 https://doi.org/10.1016/j.margen.2018.10.003
660 FAO. (2020). *The State of World Fisheries and Aquaculture 2020. In brief. Sustainability*
661 *in action.* Rome.
662 Feng, D., Li, Q., Yu, H., Kong, L., & Du, S. (2017). Identification of conserved proteins
663 from diverse shell matrix proteome in Crassostrea gigas: Characterization of
664 genetic bases regulating shell formation. *Scientific Reports*, *7*(1), 45–54.
665 https://doi.org/10.1038/srep45754
666 Fitzer, S. C., Phoenix, V. R., Cusack, M., & Kamenos, N. A. (2014). Ocean acidification
667 impacts mussel control on biomineralisation. *Scientific Reports*, *4*(1), 6218.
668 https://doi.org/10.1038/srep06218
669 Gazeau, F., Parker, L. M., Comeau, S., Gattuso, J.-P., O'Connor, W. A., Martin, S.,
670 Pörtner, H.-O., & Ross, P. M. (2013). Impacts of ocean acidification on marine

671 shelled molluscs. *Marine Biology*, *160*(8), 2207–2245.
672 https://doi.org/10.1007/s00227-013-2219-3
673 Gazeau, F., Urbini, L., Cox, T. E., Alliouane, S., & Gattuso, J.-P. (2015). Comparison of
674 the alkalinity and calcium anomaly techniques to estimate rates of net
675 calcification. *Marine Ecology Progress Series*, *527*, 1–12.
676 https://doi.org/10.3354/meps11287
677 Hazel, J. R., & Williams, E. (1990). The role of alterations in membrane lipid composition
678 in enabling physiological adaptation of organisms to their physical environment.
679 *Progress in Lipid Research*, *29*(3), 167–227. https://doi.org/10.1016/0163-
680 7827(90)90002-3
681 Hochachka, P. W., & Somero, G. (2002). Biochemical adaptation: Mechanism and
682 process in physiological evolution. *Biochemistry and Molecular Biology*
683 *Education*, *30*(3), 215–216. https://doi.org/10.1002/bmb.2002.494030030071
684 Hulbert, A. J., & Else, P. L. (1999). Membranes as possible pacemakers of metabolism.
685 *Journal of Theoretical Biology*, *199*(3), 257–274.
686 https://doi.org/10.1006/jtbi.1999.0955
687 Hüning, A. K., Melzner, F., Thomsen, J., Gutowska, M. A., Krämer, L., Frickenhaus, S.,
688 Rosenstiel, P., Pörtner, H.-O., Philipp, E. E. R., & Lucassen, M. (2013). Impacts
689 of seawater acidification on mantle gene expression patterns of the Baltic Sea blue
690 mussel: Implications for shell formation and energy metabolism. *Marine Biology*,
691 *160*(8), 1845–1861.
692 IPCC. (2019). *IPCC Special Report on the Ocean and Cryosphere in a Changing*
693 *Climate: Vol. (eds Pörtner, H. O. et al.)* (H. O. Pörtner, D. C. Roberts, V. Masson-
694 Delmotte, P. Zhai, M. Tignor, E. Poloczanska, K. Mintenbeck, A. Alegria, M.
695 Nicolai, A. Okem, J. Petzold, B. Rama, & N. M. Weyer, Eds.; H.-O. Pörtner, D.C.

696 Roberts, V. Masson-Delmotte, P. Zhai, M. Tignor, E. Poloczanska, K.
697 Mintenbeck, A. Alegría, M. Nicolai, A. Okem, J. Petzold, B. Rama, N.M. Weyer
698 (eds.)). In. press.
699 IPCC. (2021). *Climate Change 2021: The Physical Science Basis. Contribution of*
700 *Working Group I to the Sixth Assessment Report of the Intergovernmental Panel*
701 *on Climate Change: Vol. (eds Masson-Delmotte, V. P. et al.)*. Cambridge
702 University Press. In Press.
703 Klopfenstein, D. V., Zhang, L., Pedersen, B. S., Ramírez, F., Warwick Vesztrocy, A.,
704 Naldi, A., Mungall, C. J., Yunes, J. M., Botvinnik, O., Weigel, M., Dampier, W.,
705 Dessimoz, C., Flick, P., & Tang, H. (2018). GOATOOLS: A Python library for
706 Gene Ontology analyses. *Scientific Reports*, *8*(1), 10872.
707 https://doi.org/10.1038/s41598-018-28948-z
708 Knauer, J., & Southgate, P. C. (1999). A Review of the Nutritional Requirements of
709 Bivalves and the Development of Alternative and Artificial Diets for Bivalve
710 Aquaculture. *Reviews in Fisheries Science*, *7*(3–4), 241–280.
711 https://doi.org/10.1080/10641269908951362
712 Krissansen-Totton, J., Arney, G. N., & Catling, D. C. (2018). Constraining the climate
713 and ocean pH of the early Earth with a geological carbon cycle model.
714 *Proceedings of the National Academy of Sciences*, *115*(16), 4105–4110.
715 https://doi.org/10.1073/pnas.1721296115
716 Kroeker, K. J., Kordas, R. L., Crim, R., Hendriks, I. E., Ramajo, L., Singh, G. S., Duarte,
717 C. M., & Gattuso, J.-P. (2013). Impacts of ocean acidification on marine
718 organisms: Quantifying sensitivities and interaction with warming. *Global*
719 *Change Biology*, *19*(6), 1884–1896. https://doi.org/10.1111/gcb.12179

720 Langdon, C. J., & Waldock, M. J. (1981). The effect of algal and artificial diets on the
721 growth and fatty acid composition of Crassostrea gigas Spat. *Journal of the*
722 *Marine Biological Association of the United Kingdom*, *61*(2), 431–448.
723 https://doi.org/10.1017/S0025315400047056
724 Langfelder, P., & Horvath, S. (2008). WGCNA: An R package for weighted correlation
725 network analysis. *BMC Bioinformatics*, *9*, 559. https://doi.org/10.1186/1471-
726 2105-9-559
727 Lannig, G., Eilers, S., Pörtner, H. O., Sokolova, I. M., & Bock, C. (2010). Impact of
728 Ocean Acidification on Energy Metabolism of Oyster, Crassostrea gigas—
729 Changes in Metabolic Pathways and Thermal Response. *Marine Drugs*, *8*(8),
730 2318–2339. https://doi.org/10.3390/md8082318
731 Lee, H.-G., Stumpp, M., Yan, J.-J., Tseng, Y.-C., Heinzel, S., & Hu, M. Y.-A. (2019).
732 Tipping points of gastric pH regulation and energetics in the sea urchin larva
733 exposed to CO2 -induced seawater acidification. *Comparative Biochemistry and*
734 *Physiology Part A: Molecular & Integrative Physiology*, *234*, 87–97.
735 https://doi.org/10.1016/j.cbpa.2019.04.018
736 Leung, J. Y. S., Doubleday, Z. A., Nagelkerken, I., Chen, Y., Xie, Z., & Connell, S. D.
737 (2019). How calorie-rich food could help marine calcifiers in a CO2-rich future.
738 *Proceedings of the Royal Society B: Biological Sciences*, *286*(1906), 20190757.
739 https://doi.org/10.1098/rspb.2019.0757
740 Matz, M. V. (2018). Fantastic Beasts and How To Sequence Them: Ecological Genomics
741 for Obscure Model Organisms. *Trends in Genetics: TIG*, *34*(2), 121–132.
742 https://doi.org/10.1016/j.tig.2017.11.002

743 Michaelidis, B., Ouzounis, C., Paleras, A., & Pörtner, H. (2005). *Effects of long-term*
744 *moderate hypercapnia on acid-base balance and growth rate in marine mussels*
745 *(Mytilus galloprovincialis)*. *293*, 109–118. https://doi.org/10.3354/MEPS293109
746 Orr, J. C., Fabry, V. J., Aumont, O., Bopp, L., Doney, S. C., Feely, R. A., Gnanadesikan,
747 A., Gruber, N., Ishida, A., Joos, F., Key, R. M., Lindsay, K., Maier-Reimer, E.,
748 Matear, R., Monfray, P., Mouchet, A., Najjar, R. G., Plattner, G.-K., Rodgers, K.
749 B., … Yool, A. (2005). Anthropogenic ocean acidification over the twenty-first
750 century and its impact on calcifying organisms. *Nature*, *437*(7059), 681–686.
751 https://doi.org/10.1038/nature04095
752 Peck, V. L., Oakes, R. L., Harper, E. M., Manno, C., & Tarling, G. A. (2018). Pteropods
753 counter mechanical damage and dissolution through extensive shell repair. *Nature*
754 *Communications*, *9*(1), 264. https://doi.org/10.1038/s41467-017-02692-w
755 Peck, V. L., Tarling, G. A., Manno, C., Harper, E. M., & Tynan, E. (2016). Outer organic
756 layer and internal repair mechanism protects pteropod Limacina helicina from
757 ocean acidification. *Deep Sea Research Part II: Topical Studies in Oceanography*,
758 *127*, 41–52. https://doi.org/10.1016/j.dsr2.2015.12.005
759 Peñaloza, C., Gutierrez, A. P., Eöry, L., Wang, S., Guo, X., Archibald, A. L., Bean, T. P.,
760 & Houston, R. D. (2021). A chromosome-level genome assembly for the Pacific
761 oyster Crassostrea gigas. *GigaScience*, *10*(3).
762 https://doi.org/10.1093/gigascience/giab020
763 Petton, B., Boudry, P., Alunno-Bruscia, M., & Pernet, F. (2015). Factors influencing
764 disease-induced mortality of Pacific oysters Crassostrea gigas. *Aquaculture*
765 *Environment Interactions*, *6*(3), 205–222. https://doi.org/10.3354/aei00125

766 Rajan, K. C., Meng, Y., Yu, Z., Roberts, S. B., & Vengatesen, T. (2021). Oyster
767 biomineralization under ocean acidification: From genes to shell. *Global Change*
768 *Biology*, *27*(16), 3779–3797. https://doi.org/10.1111/gcb.15675
769 Rico-Villa, B., Pouvreau, S., & Robert, R. (2009). Influence of food density and
770 temperature on ingestion, growth and settlement of Pacific oyster larvae,
771 Crassostrea gigas. *Aquaculture*, *287*(3), 395–401.
772 https://doi.org/10.1016/j.aquaculture.2008.10.054
773 Schneider, C. A., Rasband, W. S., & Eliceiri, K. W. (2012). NIH Image to ImageJ: 25
774 years of image analysis. *Nature Methods*, *9*(7), 671–675.
775 https://doi.org/10.1038/nmeth.2089
776 Smith, S. V., & Key, G. S. (1975). Carbon dioxide and metabolism in marine
777 environments. *Limnology and Oceanography*, *20*(3), 493–495.
778 https://doi.org/10.4319/lo.1975.20.3.0493
779 Sokolova, I. M. (2021). Bioenergetics in environmental adaptation and stress tolerance of
780 aquatic ectotherms: Linking physiology and ecology in a multi-stressor landscape.
781 *Journal of Experimental Biology*, *224*(Suppl 1).
782 https://doi.org/10.1242/jeb.236802
783 Strader, M. E., Wong, J. M., & Hofmann, G. E. (2020). Ocean acidification promotes
784 broad transcriptomic responses in marine metazoans: A literature survey.
785 *Frontiers in Zoology*, *17*(1), 7–30. https://doi.org/10.1186/s12983-020-0350-9
786 Thomsen, J., Casties, I., Pansch, C., Körtzinger, A., & Melzner, F. (2013). Food
787 availability outweighs ocean acidification effects in juvenile Mytilus edulis:
788 Laboratory and field experiments. *Global Change Biology*, *19*(4), 1017–1027.
789 https://doi.org/10.1111/gcb.12109

790 Timmins-Schiffman, E., Coffey, W. D., Hua, W., Nunn, B. L., Dickinson, G. H., &
791 Roberts, S. B. (2014). Shotgun proteomics reveals physiological response to
792 ocean acidification in Crassostrea gigas. *BMC Genomics*, *15*(1), 951.
793 https://doi.org/10.1186/1471-2164-15-951
794 Tresguerres, M., Clifford, A. M., Harter, T. S., Roa, J. N., Thies, A. B., Yee, D. P., &
795 Brauner, C. J. (2020). Evolutionary links between intra- and extracellular acid–
796 base regulation in fish and other aquatic animals. *Journal of Experimental*
797 *Zoology Part A: Ecological and Integrative Physiology*, *333*(6), 449–465.
798 https://doi.org/10.1002/jez.2367
799 Tresguerres, M., & Hamilton, T. J. (2017). Acid–base physiology, neurobiology and
800 behaviour in relation to CO2-induced ocean acidification. *Journal of*
801 *Experimental Biology*, *220*(12), 2136–2148. https://doi.org/10.1242/jeb.144113
802 Vargas, C. A., Lagos, N. A., Lardies, M. A., Duarte, C., Manríquez, P. H., Aguilera, V.
803 M., Broitman, B., Widdicombe, S., & Dupont, S. (2017). Species-specific
804 responses to ocean acidification should account for local adaptation and adaptive
805 plasticity. *Nature Ecology & Evolution*, *1*(4), 1–7.
806 https://doi.org/10.1038/s41559-017-0084
807 Ventura, A., Schulz, S., & Dupont, S. (2016). Maintained larval growth in mussel larvae
808 exposed to acidified under-saturated seawater. *Scientific Reports*, *6*(1), 23728.
809 https://doi.org/10.1038/srep23728
810 Waldbusser, G. G., & Salisbury, J. E. (2014). Ocean Acidification in the Coastal Zone
811 from an Organism's Perspective: Multiple System Parameters, Frequency
812 Domains, and Habitats. *Annual Review of Marine Science*, *6*(1), 221–247.
813 https://doi.org/10.1146/annurev-marine-121211-172238

814 Wang, X., Wang, M., Jia, Z., Song, X., Wang, L., & Song, L. (2017). A shell-formation
815 related carbonic anhydrase in Crassostrea gigas modulates intracellular calcium
816 against CO2 exposure: Implication for impacts of ocean acidification on mollusk
817 calcification. *Aquatic Toxicology*, *189*, 216–228.
818 https://doi.org/10.1016/j.aquatox.2017.06.009
819 Wang, X., Wang, M., Wang, W., Liu, Z., Xu, J., Jia, Z., Chen, H., Qiu, L., Lv, Z., Wang,
820 L., & Song, L. (2020). Transcriptional changes of Pacific oyster Crassostrea gigas
821 reveal essential role of calcium signal pathway in response to CO2-driven
822 acidification. *The Science of the Total Environment*, *741*, 140177.
823 https://doi.org/10.1016/j.scitotenv.2020.140177
824 Wood, S. N. (2001). Minimizing Model Fitting Objectives That Contain Spurious Local
825 Minima by Bootstrap Restarting. *Biometrics*, *57*(1), 240–244.
826 https://doi.org/10.1111/j.0006-341X.2001.00240.x
827 Wright, J. M., Parker, L. M., O'Connor, W. A., Scanes, E., & Ross, P. M. (2018). Ocean
828 acidification affects both the predator and prey to alter interactions between the
829 oyster Crassostrea gigas (Thunberg, 1793) and the whelk Tenguella marginalba
830 (Blainville, 1832). *Marine Biology*, *165*(3), 46. https://doi.org/10.1007/s00227-
831 018-3302-6
832 Yan, L., Li, Y., Wang, Z., Su, J., Yu, R., Yan, X., Ma, P., & Cui, Y. (2018). Stress
833 response to low temperature: Transcriptomic characterization in Crassostrea
834 sikamea × Crassostrea angulata hybrids. *Aquaculture Research*, *49*(10), 3374–
835 3385. https://doi.org/10.1111/are.13801
836 Zhao, X., Han, Y., Chen, B., Xia, B., Qu, K., & Liu, G. (2020). CO2-driven ocean
837 acidification weakens mussel shell defense capacity and induces global molecular

838 compensatory responses. *Chemosphere*, *243*, 125415.
839 https://doi.org/10.1016/j.chemosphere.2019.125415
840

841 **Figure captions**

842 **Figure 1.** Oysters exposed to 15 pH conditions for 23 d. Five oysters were selected from
843 each condition, and sorted from the smallest to the biggest. Corresponding pH (total scale)
844 and saturation states of seawater with respect to calcite (Ω_{CA}) are shown.

845 **Figure 2.** Biometry and physiological rates of oysters as a function of pH (total scale).
846 (A) shell length, (B) shell thickness, (C) shell weight, (D) growth rate in shell length, (E)
847 growth rate in total body weight (TW), (F) dry flesh weight, (E) net calcification rate, (H)
848 ingestion rate and (I) respiration rate. Data are means ± SD when available. Tipping points
849 and critical points and their 95% confidence intervals are shown in grey and red,
850 respectively. The significance levels of the slopes are presented using symbols (P< 0.001
851 ***, < 0.01 **, < 0.05 *, < 0.1 ·).

852 **Figure 3.** Membrane fatty acid (FA) composition of oysters as a function of pH (total
853 scale). (A) Principal component analysis of polar fatty acid classes for oysters (n = 15
854 pools of five oysters) exposed to 15 pH levels. Arrows represent fatty acids contributing
855 to more than 5% of the first principal component (PC1). Individuals are colored according
856 to the average pH. Contribution to membrane of the sum of fatty acids that are (B)
857 positively or (C) negatively correlated to PC1 as a function of pH. Tipping points and
858 their 95% confidence intervals are shown in grey. The significance levels of the slopes
859 are presented using symbols (P < 0.001 ***, < 0.01 **, < 0.05 *, < 0.1 ·).

860 **Figure 4.** Tipping points of oyster transcriptome. (A-C) Frequency distribution of
861 tipping-point for piecewise linear relationships (left side). Linear and loglinear models
862 (no tipping-point) are under "Lin" name. Genes are grouped into three clusters of genes
863 that co-vary together. The grey line indicates the distribution frequency of all genes
864 irrespective of clusters. Groups of genes which exhibit neighboring tipping points with
865 distribution frequencies > 5% (shown as a dotted line), were grouped together. The

866 segments above the bars indicate the groups of genes on which GO analyses were
867 conducted. In each case, the gene that best represents the cluster according to module
868 membership, gene significance for pH and R^2 is presented as a function of pH as an
869 example (right side). Tipping points and their 95% confidence intervals are shown in
870 grey. The significance levels of the slopes are presented using stars (P <0.001 ***, p<0.01
871 **, p<0.05 *). Gene names are: LOC117690205: monocarboxylate transporter 12-like,
872 LOC105317113: 60S ribosomal protein L10a, LOC105331560: protocadherin Fat 4
873 **Figure 5.** Graphical summary of the reaction norm of juvenile oysters *Crassostrea gigas*
874 over a wide range of pH conditions. Abbreviations: GO, gene ontology term; ARA,
875 arachidonic acid, EPA, ecosapentaenoic acid, DHA, docosahexaenoic acid, NMI, non-
876 methylene interrupted.

877

878 **Figures**

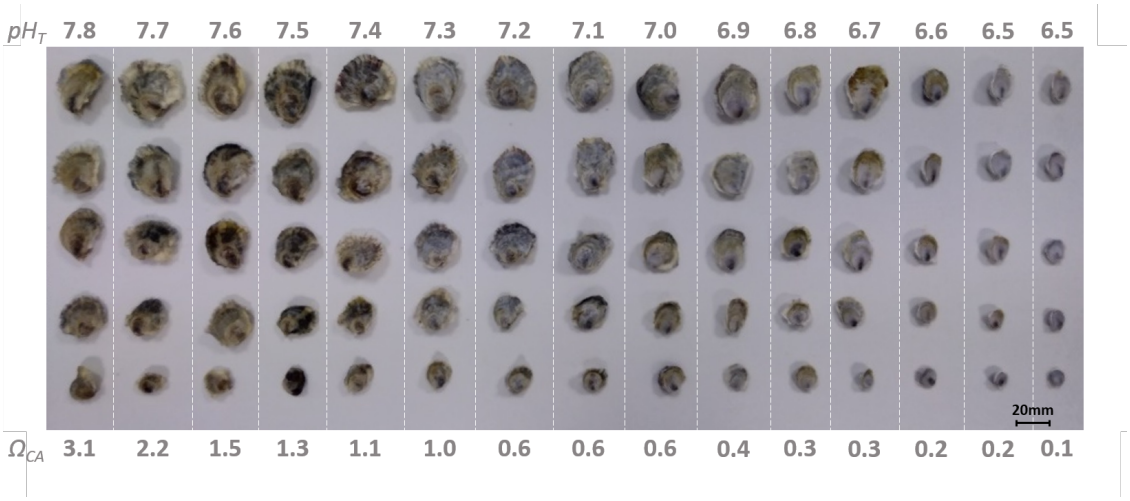

879

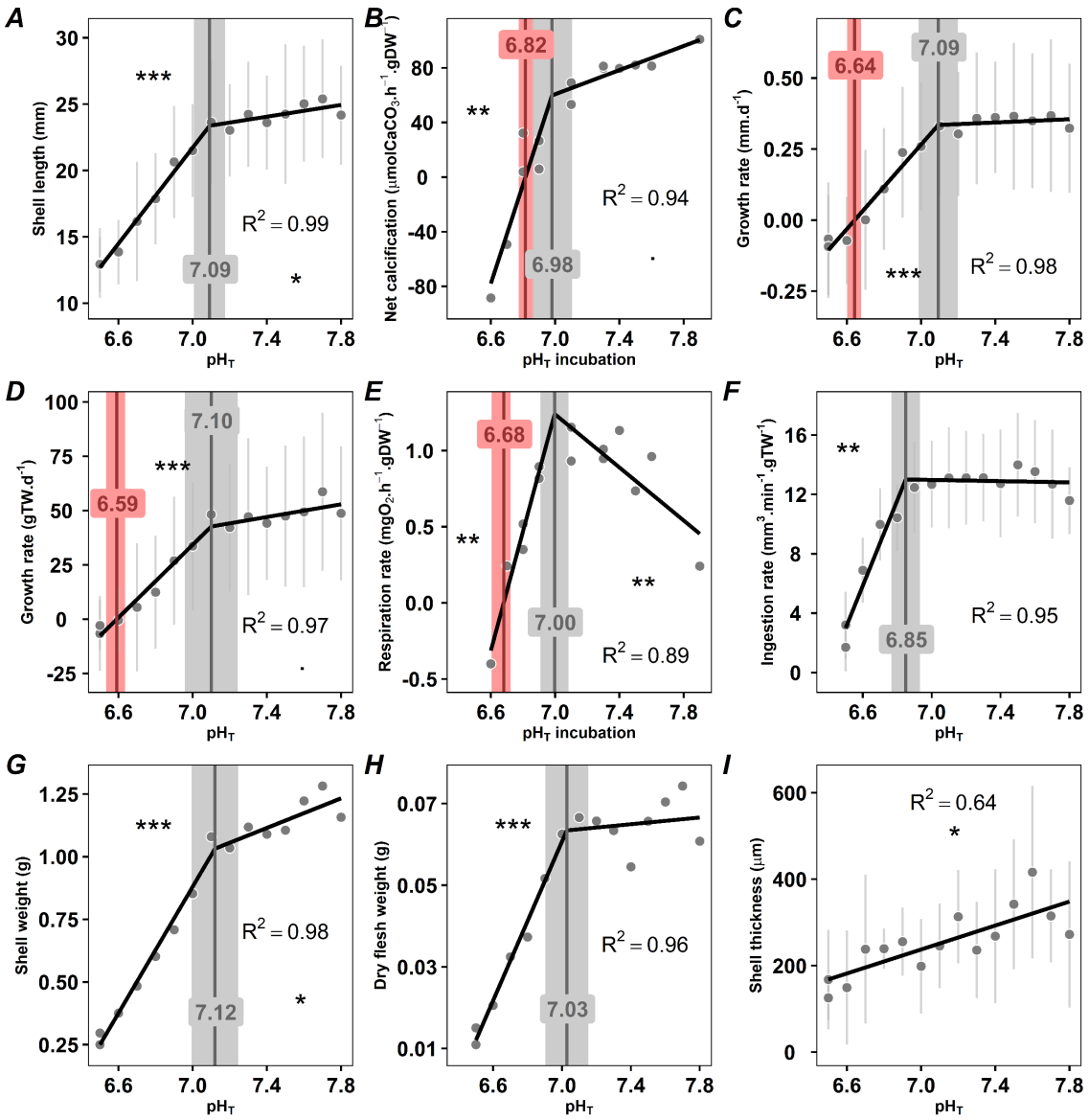

880

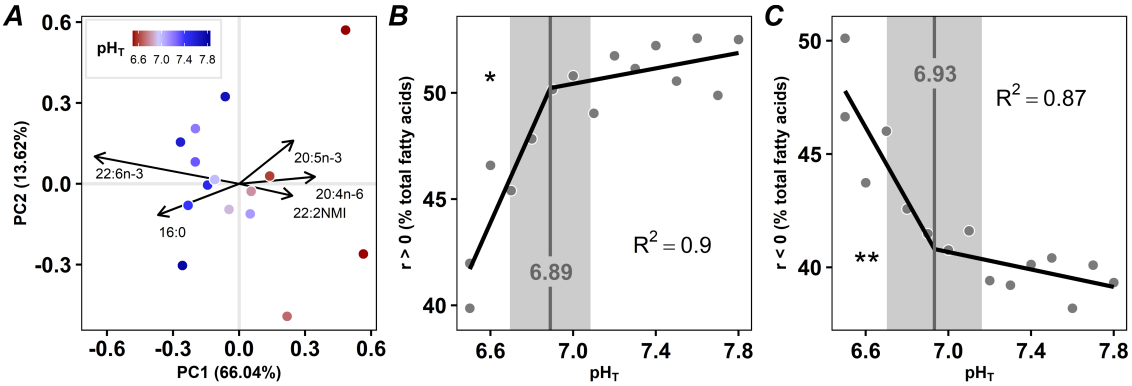

881

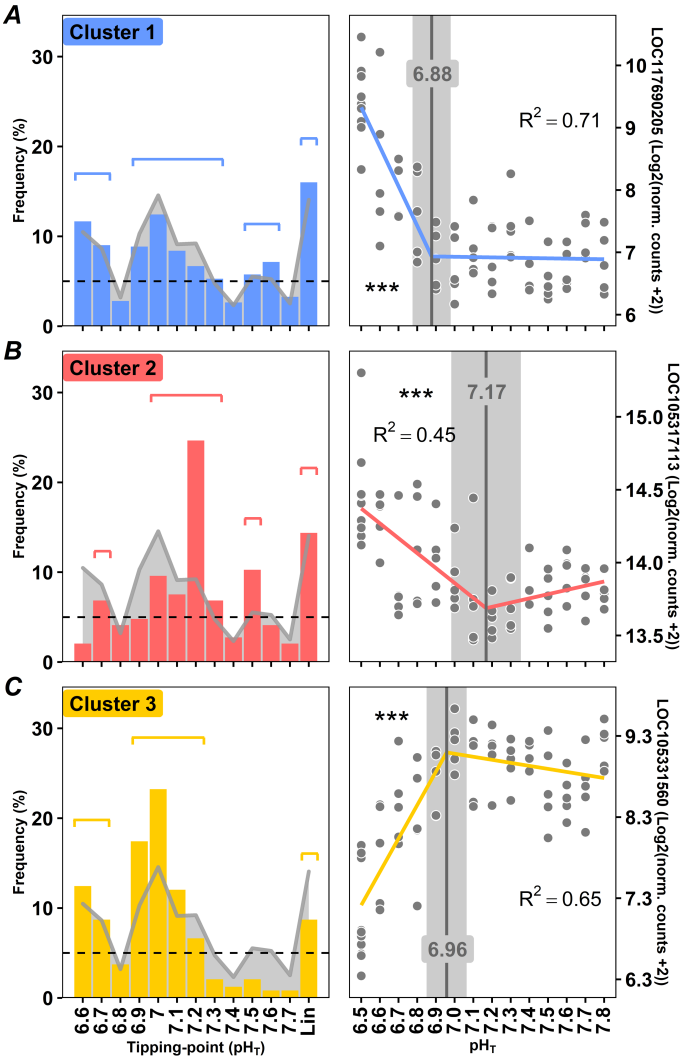

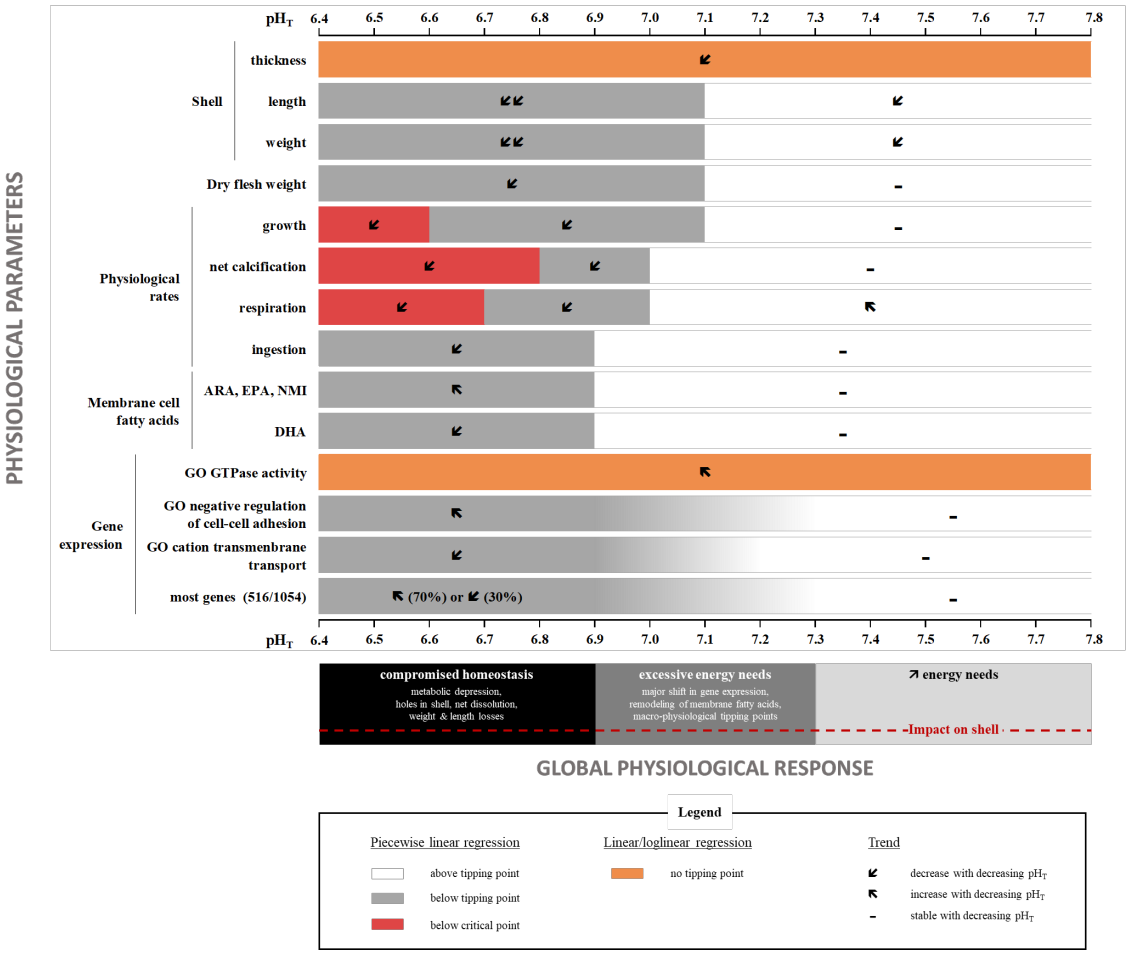

Table 1 Gene ontology term enrichment and tipping point. Model characteristics, physiological function and gene ontology for each cluster. For each GO term, the P-value of Bonferroni test is displayed using symbols (P < 0.001 ***, < 0.01 **, < 0.05 *, < 0.1 ·). Abbreviations: TP: tipping point

Cluster	Models			Physiological function	Gene Ontlogy			
	shape of the relationship	*TP range*	*number of genes*		*GO*	*name*	*number of genes*	*p bonferroni*
1	↖←	6.9-7.3	283	regulation of RNA-transcription	.....GO:1903506	regulation of nucleic acid-templated transcription	38	**
					.....GO:0006357	regulation of transcription by RNA polymerase II	30	***
				cellular metabolism & macromolecule byosynthesis	.....GO:2000112	regulation of cellular macromolecule biosynthetic process	41	*
					.....GO:0031325	positive regulation of cellular metabolic process	39	*
				cell-cell adhesion	.....GO:0022408	negative regulation of cell-cell adhesion	8	•
	↖	n.a.	96	GTP metabolism	.....GO:0003924	GTPase activity	8	**
					.....GO:0005525	GTP binding	9	*
				ribonucleotide metabolism	.....GO:0032561	guanyl ribonucleotide binding	9	•
					.....GO:0032550	purine ribonucleoside binding	9	•
2	↖←	7.0-7.3	62	ribosome synthesis / ribosomal subunit assembly	.....GO:0000027	ribosomal large subunit assembly	4	**
					.....GO:0022625	cytosolic large ribosomal subunit	10	***
					.....GO:0022627	cytosolic small ribosomal subunit	6	***
					.....GO:0022618	ribonucleoprotein complex assembly	6	*
				RNA-binding	.....GO:1990932	5.8S rRNA binding	3	***
					.....GO:0019843	rRNA binding	8	***
					.....GO:0003729	mRNA binding	6	*
				translation	.....GO:0002181	cytoplasmic translation	8	***

				protein & amino acids synthesis	.....GO:0043604	amide biosynthetic process	25	***
					.....GO:0043043	peptide biosynthetic process	25	***
				ribosome synthesis / ribosomal subunit assembly	.....GO:0022627	cytosolic small ribosomal subunit	3	**
					.....GO:0022625	cytosolic large ribosomal subunit	6	***
	↖	n.a.	25	translation	.....GO:0006412	translation	10	***
				RNA processing	.....GO:0006364	rRNA processing	4	•
				protein & amino acids synthesis	.....GO:0043043	peptide biosynthetic process	10	***
					.....GO:0043604	amide biosynthetic process	11	***
3					....GO:0006811	ion transport	19	**
	↙↙	6.9-7.2	150	ion transport	....GO:0022890	inorganic cation transmembrane transporter activity	14	*
					....GO:0008324	cation transmembrane transporter activity	14	•

Table 2 Tipping points of genes related to calcification and production of the shell organic matrix. Model characteristics and physiological function are reported for each gene. The slope inclination is displayed using arrows only if it is significant according to Student t tests ($P < 0.05$). Abbreviations: TP: tipping point, CBP*: calcium-binding proteins,* ACCBP: *amorphous calcium carbonate-binding proteins*, SMP: *shell matrix proteins.*

Physiological function		**Model**					**Gene**	
		Model	*TP*	*Slope before TP*	*Slope after TP*	R^2	*Cluster*	*Name*
Calcification	*Ion transport*	piecewise	6.6±0.1	↖	n.s.	0.33	1	sodium-dependent phosphate transport protein 2B
			6.6±0.0	↖	n.s.	0.37	1	monocarboxylate transporter 5
	CBP		6.6±0.0	↖	n.s.	0.20	1	fibrillin-2-like
			6.6±0.0	↙	n.s.	0.48	3	EF-hand Ca-binding domain-containing protein 6
	Ca^{2+} signaling pathway		6.7±0.2	n.s.	↖	0.20	2	neurocalcin-delta
	CBP		6.7±0.1	↙	n.s.	0.32	3	ankyrin repeat and EF-hand domain-containing protein 1
	Ca^{2+} signaling pathway		6.8±0.1	↙	n.s.	0.40	3	polycystin-2
			6.9±0.3	n.s.	↖	0.09	1	neurocalcin-like protein
	Ion transport		6.9±0.1	↖	n.s.	0.71	1	monocarboxylate transporter 12-like
	CBP		6.9±0.1	↙	n.s.	0.17	3	D-galactoside-specific lectin
			6.9±0.1	↙	n.s.	0.31	3	sarcoplasmic calcium-binding protein
			6.9±0.1	↙	n.s.	0.42	3	calmodulin-like protein 12
	Ion transport		6.9±0.1	↙	↙	0.45	3	sodium/calcium exchanger 3
	ACCBP		6.9±0.1	↙	n.s.	0.49	3	neuronal acetylcholine receptor subunit alpha-6
			6.9±0.1	↙	n.s.	0.36	3	acetylcholine receptor subunit beta
			6.9±0.1	↙	n.s.	0.31	3	neuronal acetylcholine receptor subunit alpha-3
	Ca^{2+} signaling pathway		7.0±0.2	↖	n.s.	0.17	1	metabotropic glutamate receptor 5
	Signaling pathway		7.0±0.2	↖	n.s.	0.30	1	toll-like receptor 4
	Ion transport		7.0±0.2	n.s.	↖	0.19	1	G protein-activated inward rectifier potassium channel 2
			7.0±0.4	n.s.	↖	0.15	1	monocarboxylate transporter 9
			7.0±0.1	↙	n.s.	0.29	3	organic cation transporter protein
			7.0±0.1	↙	n.s.	0.32	3	small conductance calcium-activated potassium channel protein 2
			7.0±0.1	↙	n.s.	0.24	3	sodium/glucose cotransporter 4

	Ca^{2+} signaling pathway		7.0±0.1	↙	n.s.	0.65	3	protocadherin FAT 4
	ACCBP		7.0±0.1	↙	n.s.	0.43	3	acetylcholine receptor subunit beta-type unc-29
	CBP		7.1±0.3	↖	n.s.	0.28	1	neurogenic locus notch homolog protein 1
	Ca^{2+} signaling pathway		7.1±0.2	↖	n.s.	0.26	1	protocadherin gamma-A4
	CBP		7.1±0.1	↙	↙	0.42	3	delta-like protein 4 / delta-like protein C
	Ion transport		7.1±0.1	↙	n.s.	0.28	3	calcium-activated potassium channel slowpoke
	Ca^{2+} signaling pathway		7.2±0.1	↖	n.s.	0.18	1	protocadherin-11 X-linked
			7.2±0.2	↙	n.s.	0.14	3	cadherin-87A
	Ion transport		7.3±0.2	↖	n.s.	0.20	1	monocarboxylate transporter 12-like
	CBP		7.4±0.1	↖	n.s.	0.29	1	calmodulin-A
	Ca^{2+} signaling pathway		7.5±0.1	↖	n.s.	0.21	1	protocadherin gamma-B1
	Ion transport		7.6±0.1	↖	↖	0.33	1	potassium channel GORK
		loglinear	n.a.	↖	n.a.	0.42	1	monocarboxylate transporter 9-like
	CBP		n.a.	↙	n.a.	0.25	3	fibrillin-1
Shell organic matrix & periostracum	*SMP*	piecewise	6.6±0.0	↖	↖	0.66	1	asparagine-rich protein
			7.0±0.1	↖	n.s.	0.21	1	perlucin-like protein
	SMP, periostracum formation		7.0±0.1	↙	n.s.	0.37	3	putative tyrosinase-like protein tyr-1
			7.1±0.2	↖	n.s.	0.20	1	tyrosinase-like protein 2
			7.4±0.2	↖	n.s.	0.24	1	tyrosinase-like protein 2
			7.4±0.2	↖	n.s.	0.30	1	tyrosinase-like protein 2
	SMP, carbonic anhydrase		7.5±0.2	↖	n.s.	0.19	1	nacrein-like protein F2
			7.5±0.2	↖	n.s.	0.25	1	nacrein-like protein / carbonic anhydrase 6
	SMP	loglinear	n.a.	↙	n.a.	0.23	3	leucine-rich repeat and fibronectin type-III domain-containing protein 5-like
	SMP, periostracum formation		n.a.	↖	n.a.	0.43	1	tyrosinase-like protein 1
	SMP		n.a.	↖	n.a.	0.28	1	circumsporozoite protein-like